Article

The Activation of Methane on Ru, Rh, and Pd Decorated Carbon Nanotube and Boron Nitride Nanotube: A DFT Study

Bundet Boekfa [1,2,*], Piti Treesukol [1,2], Yuwanda Injongkol [1,2], Thana Maihom [1,2], Phornphimon Maitarad [3] and Jumras Limtrakul [4]

[1] Department of Chemistry, Faculty of Liberal Arts and Science, Kasetsart University, Kamphaengsaen Campus, Nakhonpathom 73140, Thailand; faasptt@ku.ac.th (P.T.); yuwanda.in@ku.th (Y.I.); faastnm@ku.ac.th (T.M.)

[2] Center for Advanced Studies in Nanotechnology for Chemical, Food and Agricultural Industries, KU Institute for Advanced Studies, Kasetsart University, Bangkok 10900, Thailand

[3] Research Center of Nanoscience and Technology, Shanghai University, Shanghai 200444, China; pmaitarad@shu.edu.cn

[4] Department of Materials Science and Engineering, Vidyasirimedhi Institute of Science and Technology, Rayong 21210, Thailand; jumras.limtrakul@vistec.ac.th

* Correspondence: bundet.b@ku.ac.th; Tel.: +66-86-555-4089

check for updates

Abstract: Methane decomposition catalyzed by an Ru, Rh, or Pd atom supported on a carbon or boron nitride nanotubes was analyzed by means of the density functional theory with the M06-L hybrid functional. The results suggested that the dissociative reaction of methane was a single-step mechanism. Based on the calculated activation energy, the Ru-decorated carbon nanotube showed superior catalytic activity with an activation barrier of 14.5 kcal mol^{-1}, followed by the Rh-decorated carbon nanotube (18.1 kcal mol^{-1}) and the Pd-decorated carbon nanotube (25.6 kcal mol^{-1}). The catalytic performances of metals supported on a boron nitride nanotube were better than those on a carbon nanotube. The total activation barrier for the Ru, Rh, and Pd atoms on boron nitride nanotube was 10.2, 14.0, and 20.5 kcal mol^{-1}, respectively. Dissociative adsorption complexes on the Ru–boron nitride nanotube were the most stable. The anionic state of the supported metal atom was responsible for decreasing the activation energy of methane decomposition. Our finding provides a crucial point for further investigation.

Keywords: methane decomposition reaction; carbon nanotubes; boron nitride nanotubes; density functional theory

1. Introduction

Methane is one of the most important raw materials in the chemical industry. The methane to olefin (MTO), dehydro-halogenative coupling (DHHC), and oxidative coupling of methane (OCM) have been intensely investigated as promising sources of renewable energy [1,2]. Many research groups have focused on the methane dissociation step, which is the rate-determining step for many oxidative reactions. They have also suggested that dissociation of strong C–H bonds in methane can be achieved by the use of various catalysts [2–11].

Metal particles supported on carbon materials, such as nanotubes and graphene, are a promising type of catalyst for methane dissociation due to the synergistic effect between the activity of the metal particle itself and the metal–support interaction [12–15]. Recently, various metal particles, such as Pt, Pd, Ru, Ag, Au, and Ge, have been reported as effective catalysts on carbon nanotubes (CNT)

due to their high activity and durability [16–20]. Supported Pd, Pt, Rh, and Au particles were used for the detection of H_2, CH_4, CO, and H_2S gases [17,21–23], and as a catalyst for NO_x reduction [24]. Moreover, the dissociation of methane catalyzed by various transition metals (Ni, Rh, Co, Ru, Pd, Pt, Ir, Cu, and Au) on graphene has also been reported [25].

Critical understanding of supported metal catalysts can be obtained by means of theoretical methods. Density functional theory (DFT) has high credibility for the adsorption and reactions of small molecules on metal-doped carbon nanotubes. Direct oxidation of methane to methanol on Fe–O-modified graphene was studied by DFT with PBE-D2 functional and the calculated activation energy of 17.5 kcal mol^{-1} was required for the first step of methane dissociation [7]. The activation energy for methane decomposition on a periodic Rh metal was calculated to be 16.6 kcal mol^{-1} by DFT with GGA/PW91 functionals [26]. The oxygen evolution reaction on iron oxide nanoclusters under confinement of (7,7) and (8,8) armchair carbon nanotube was studied with DFT [27]. The adsorption of methane and biogas on the surface of pyridine-like, nitrogen-doped graphene decorated with Rh, Pt, and Pd was calculated with a PBE functional [28]. The adsorption of hydrogen on an Rh-decorated carbon nanotube (8,0) was examined by DFT with a PBE functional and it was found that a Rh particle increased the binding energy compared to the pristine nanotube [29]. Although carbon nanotubes with various metal particles have been demonstrated to be good catalysts for methane dissociation, a boron nitride nanotube (BNNT) was reported to be an outstanding support for various metal particles as well [30].

The application of Ru, Rh, and Pd as catalysts for C–C bond formation and C–H bond activation was previously reviewed in detail [31]. To understand the mechanism of the catalyzed methane dissociation, more information was required at a molecular level. In this work, DFT with well-defined M06-L functional [32] was utilized to calculate adsorption structures, related species, and transition state complexes. The primary aim of this study was to investigate the catalytic properties of Ru, Rh, and Pd metal decorated on carbon nanotubes versus those on boron nitride nanotubes for the methane dissociative reaction.

2. Results

The activations of methane on transition metal-decorated carbon nanotubes and boron nitride nanotubes were examined by DFT calculation with M06-L functional. The $C_{96}H_{16}$ and $B_{48}N_{48}H_{16}$ clusters generated from the carbon nanotube unit cell were optimized. For the $C_{96}H_{16}$ cluster, the average C–C bond distance was determined to be 1.42 Å, which was close to the experimental observation of 1.44 Å [33]. The average B–N bond distance of the $B_{48}N_{48}H_{16}$ cluster was calculated to be 1.44 Å, which was slightly longer than the C–C bond of the carbon nanotube cluster. While electron density was distributed equally throughout the carbon nanotube, the Mulliken charges on boron and nitrogen were +0.5|e| and −0.5|e|, respectively.

The optimized structures for a metal-decorated carbon nanotube and boron nitride nanotube are illustrated in Figure 1. The optimized parameters are shown in Tables S1 and S2 in the supporting information. The most stable states for the Ru–, Rh– and Pd–$C_{96}H_{16}$ clusters were triplet, doublet, and triplet, respectively. Ru and Rh atoms were bound to the carbon nanotube over the π bond of the C–C of a hexagonal ring, with the two shortest M–C bond distances of 2.13 Å/2.14 Å for Ru and 2.06 Å/2.14 Å for Rh. On the other hand, the Pd atom was bound to the C–C bridge of the tube with two identical Pd–C bonds of 2.16 Å. The most stable configurations for the Ru- and Rh-decorated boron nitride nanotubes were in the same spins as the metal-decorated carbon nanotubes. The most stable state for the Pd-decorated boron nitride nanotubes was the singlet state. The metal atom adsorbed on top of the hexagonal ring of the tube with B–M and N–M bond distances of 2.24 Å/2.17 Å for Ru, and 2.22 Å/2.14 Å for Rh. For the Pd–$B_{48}N_{48}H_{16}$, a Pd atom was bound to a B–N bridge with B–Pd and N–Pd distances of 2.23 Å and 2.21 Å, respectively. We found that the charge transfer observed in metal/carbon nanotube systems was quite different from that observed in metal/boron nitride nanotube systems. The partial charges on the supported Ru, Rh, and Pd atoms were quite positive on

carbon nanotubes (0.44 |e|, 0.32 |e| and 0.22 |e|) but slightly negative on boron nitride nanotubes (−0.05 |e|, −0.12 |e| and −0.14 |e|).
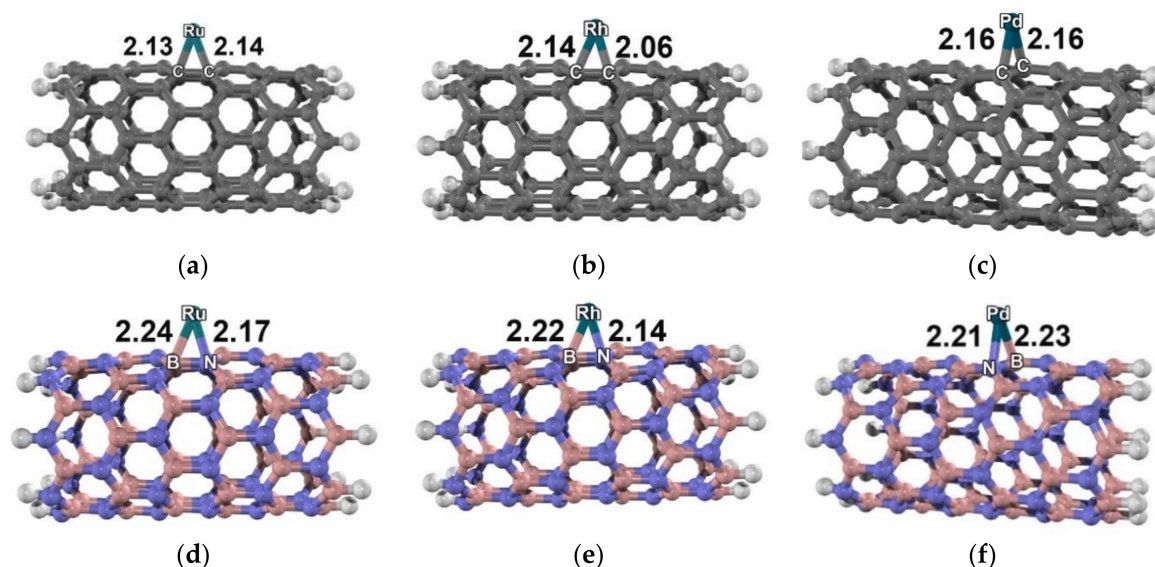
Figure 1. Optimized molecular structure of (**a**) Ru–, (**b**) Rh– and (**c**) Pd–carbon nanotubes; (**d**) Ru–, (**e**) Rh– and (**f**) Pd–boron nitride nanotubes with M06-L functional. Distances are in Å.

The mechanisms of methane dissociation on each supported metal were found to be quite similar. Therefore, only the methane dissociation on the Ru–$C_{96}H_{16}$ and Ru–$B_{48}N_{48}H_{16}$ clusters is discussed in detail. The reactions on both clusters with triplet state and no spin crossing were analyzed. For the Ru–$C_{96}H_{16}$ cluster, a methane was adsorbed on top of the supported Ru atom with two symmetric H···Ru distances [AD1, Figure 2a]. The C–Ru distance of the methane/Ru–$C_{96}H_{16}$ cluster was 2.11 Å and the calculated adsorption energy was −12.0 kcal mol^{-1}. Upon adsorption, C–H bonds of the methane were enlarged for 0.2 Å. Moreover, the structure at the adsorption site of the carbon nanotube was slightly disturbed. The C–H bond breaking was proposed to be a concerted process, as confirmed by the transition state calculation. At the transition state [TS1, Figure 2b], the Ru–C bond and Ru–H bond were forming while one of the C–H bonds was breaking with a single imaginary frequency at 650i cm^{-1}. The Ru···C, Ru···H and C–H bond distances of the transition state were 2.12, 1.63, and 1.58 Å, respectively. The intermediate product of this step was a dissociative adsorption of methane on the Ru atom [DA1, Figure 2c]. Ru–C and Ru–H bond lengths of the dissociative form were 2.05 and 1.64 Å, respectively. The relative energy for the dissociative adsorption complex was −3.6 kcal mol^{-1} with an activation energy of 14.5 kcal mol^{-1}.

For the Ru–$B_{48}N_{48}H_{16}$ cluster, a methane was adsorbed on the Ru atom with an adsorption energy of −14.8 kcal mol^{-1} [AD2, Figure 2d]. Compared to Ru–$C_{96}H_{16}$, more negative adsorption energy of a methane on Ru–$B_{48}N_{48}H_{16}$ corresponded to a shorter Ru···H distance (2.09 Å). At the transition state [TS2, Figure 2e], methane was activated over the Ru–$B_{48}N_{48}H_{16}$ nanotube with Ru···C, Ru···H and C–H bond distances of 2.10, 1.63, and 1.55 Å, respectively. The dissociative adsorption of methane [IN2, Figure 2f], on the Ru atom was 17.8 kcal mol^{-1} exothermic with the activation barrier of 10.2 kcal mol^{-1}. The $B_{48}N_{48}H_{16}$ nanotube cluster was found to be capable of donating an electron to the Ru atom. The change of charge of the Ru atom on boron nitride from −0.17 |e| in AD to +0.11 |e| in DA significantly altered the mechanism.
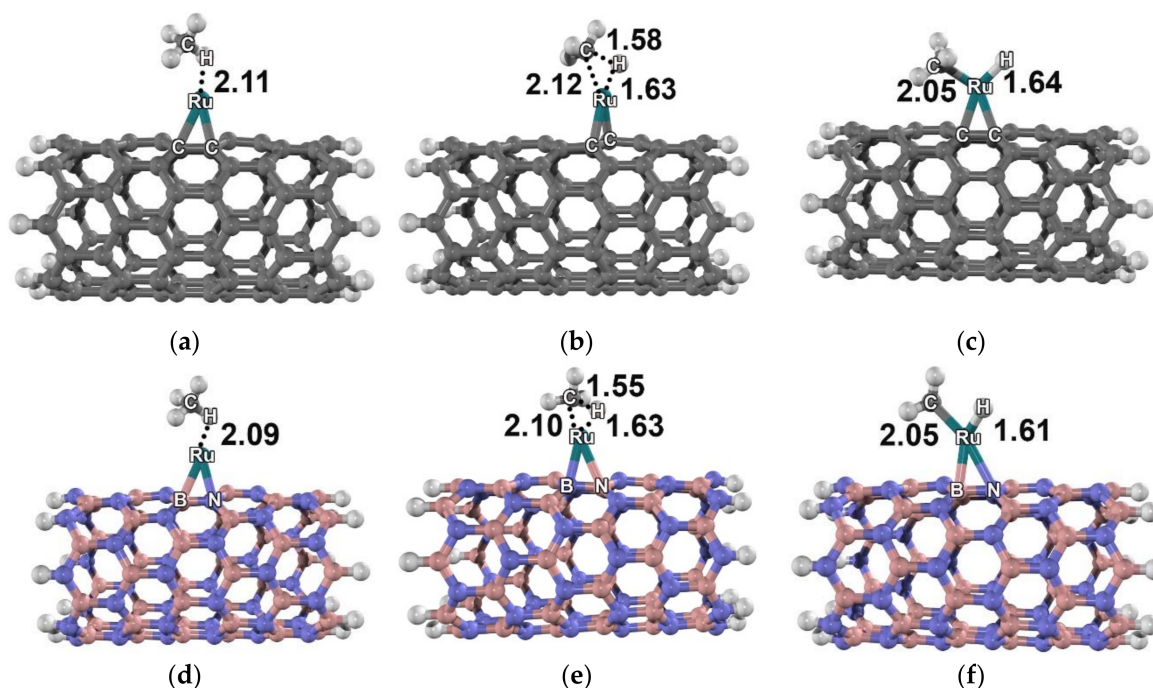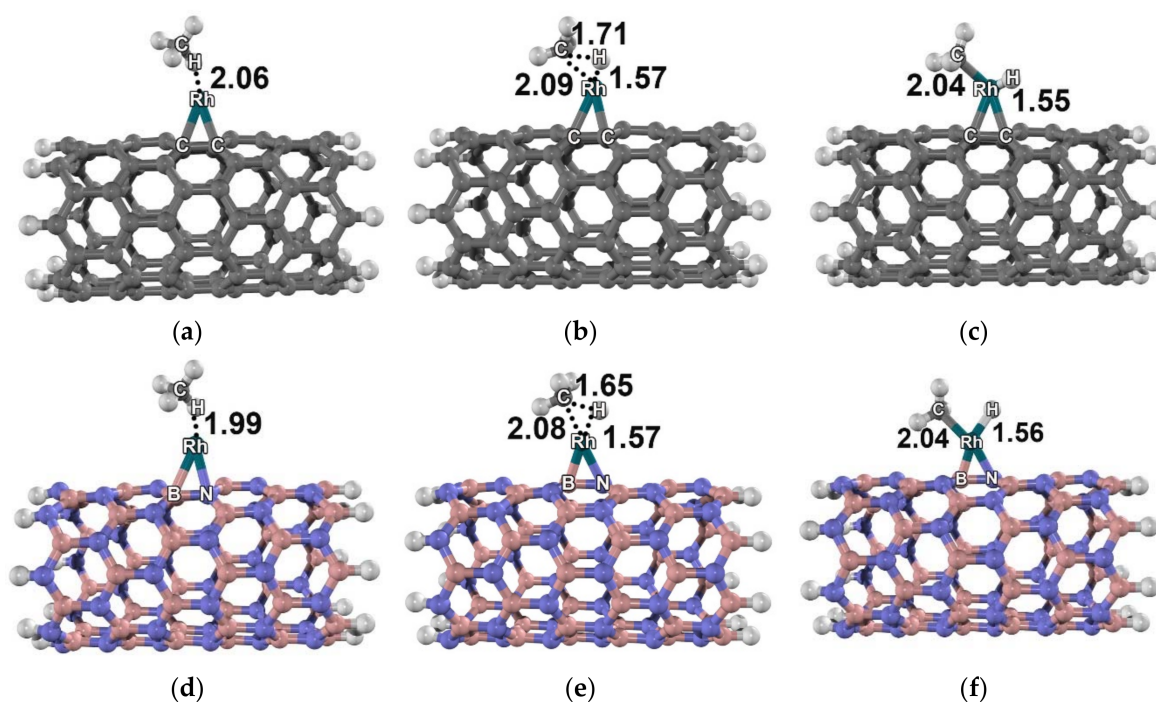
Figure 2. Molecular structure of the methane dissociative adsorption reaction: (**a**) ^{3}AD1, (**b**) ^{3}TS1, and (**c**) ^{3}DA1 on the Ru–carbon nanotube; (**d**) ^{3}AD2, (**e**) ^{3}TS2, and (**f**) ^{3}DA2 on the Ru–boron nitride nanotube. Distances are in Å.

All structures related to reactions on the Rh–$C_{96}H_{16}$, Pd–$C_{96}H_{16}$, Rh–$B_{48}N_{48}H_{16}$ and Pd–$B_{48}N_{48}H_{16}$ clusters are shown in Figures 3 and 4. Both the reactions on Rh–$C_{96}H_{16}$ and on Rh–$B_{48}N_{48}H_{16}$ proceeded with doublet multiplicity. For the Pd–$C_{96}H_{16}$ cluster, the reaction was found to be in quintet state, while the reaction on the Pd–$B_{48}N_{48}H_{16}$ cluster was in singlet state. All energy profiles are shown in Figure 5.

The adsorption energies of the methane on Ru–, Rh–, and Pd–$C_{96}H_{16}$ were −12.0, −11.2, and −11.7 kcal mol^{-1}, respectively. The corresponding actual activation energies were 14.5, 18.1, and 25.6 kcal mol^{-1}, respectively. For the carbon nanotube, the adsorption energy and activation energy of methane were in the order Ru–$C_{96}H_{16}$ > Rh–$C_{96}H_{16}$ > Pd–$C_{96}H_{16}$. Methane on a boron nitride nanotube possessed higher adsorption energies than on a carbon nanotube. The adsorption energies were −14.8, −14.3, and −13.3 kcal mol^{-1} for Ru–, Rh–, and Pd–$B_{48}N_{48}H_{16}$, respectively. The same adsorption trend was found for the adsorption of methane on the decorated, nitrogen-doped graphene of the Rh and Pd of −25.3 and −23.0 kcal mol^{-1}, respectively [28]. The Metal⋯H intermolecular bond distances of the adsorption on the Ru–, Rh–, and Pd–boron nitride nanotube were shorter than those on the Ru–, Rh–, and Pd–carbon nanotube, which corresponded to the higher adsorption energies. The actual activation energies were 10.2, 14.0, and 20.5 kcal mol^{-1} for the reaction on Ru–, Rh–, and Pd–$B_{48}N_{48}H_{16}$, respectively, which were found to be lower than those of the carbon nanotube systems reported above. The reason might be due to the shorter C–H bond distances in transition states of the boron nitride systems, leading to an earlier transition state compared to the carbon nanotube ones (see Figures 2–4).

The activation energies for the methane activation on the Ru– and Rh–carbon nanotube and boron nitride nanotubes from this study were lower than those on Fe–graphene (17.5 kcal mol^{-1} from a previous calculation) [7]. The methane activations on Au-supported zeolites were reported to be 12.7 and 14.0 kcal mol^{-1} for Au-FER and Au-MCM-22 [3], respectively. The methane activation energy on an Ru–boron nitride nanotube of 10.2 kcal mol^{-1} is comparable to the experimentally determined

activation energy of 5.9–7.0 kcal mol^{-1} on silica-supported Ru [34] and 7.0 kcal mol^{-1} on rhodium surfaces [35].

Figure 3. Molecular structure of the methane dissociative adsorption reaction: (**a**) ^{2}AD3, (**b**) ^{2}TS3, and (**c**) ^{2}DA3 on the Rh–carbon nanotube; (**d**) ^{2}AD4, (**e**) ^{2}TS4, and (**f**) ^{2}DA4 on the Rh–boron nitride nanotube. Distances are in Å.
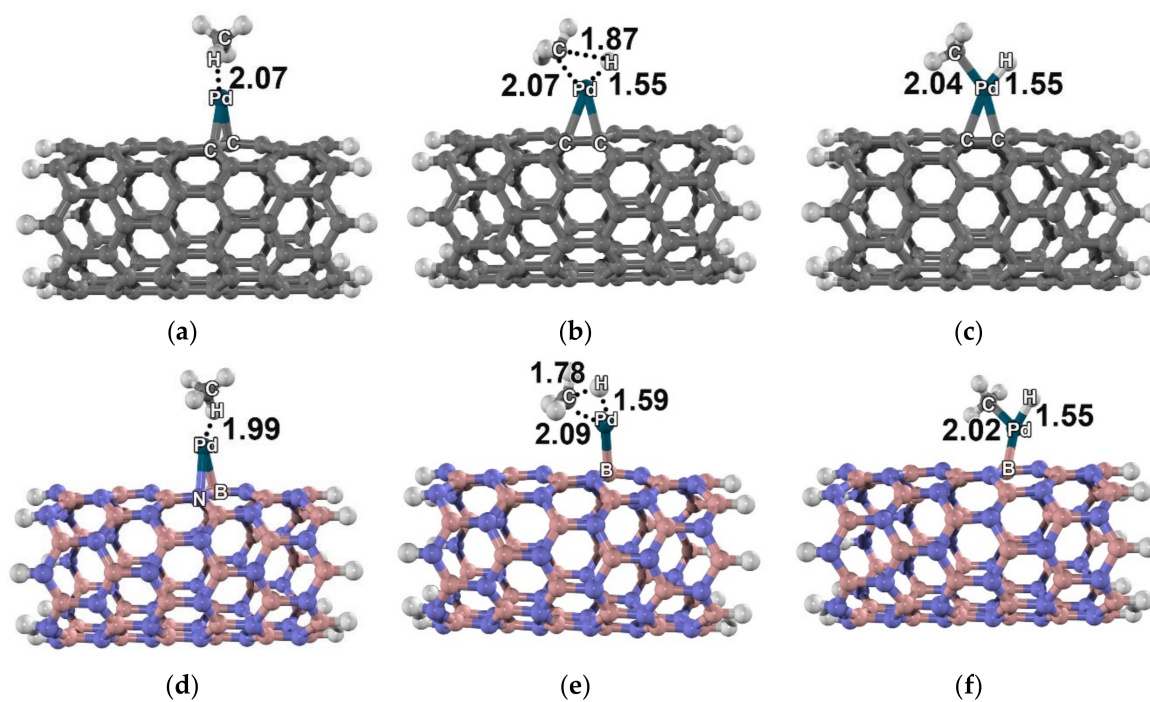
Figure 4. Molecular structure of the methane dissociative adsorption reaction: (**a**) ^{5}AD5, (**b**) ^{5}TS5, and (**c**) ^{5}DA5 on the Pd–carbon nanotube; (**d**) ^{1}AD6, (**e**) ^{1}TS6, and (**f**) ^{1}DA6 on the Pd–boron nitride nanotube. Distances are in Å.
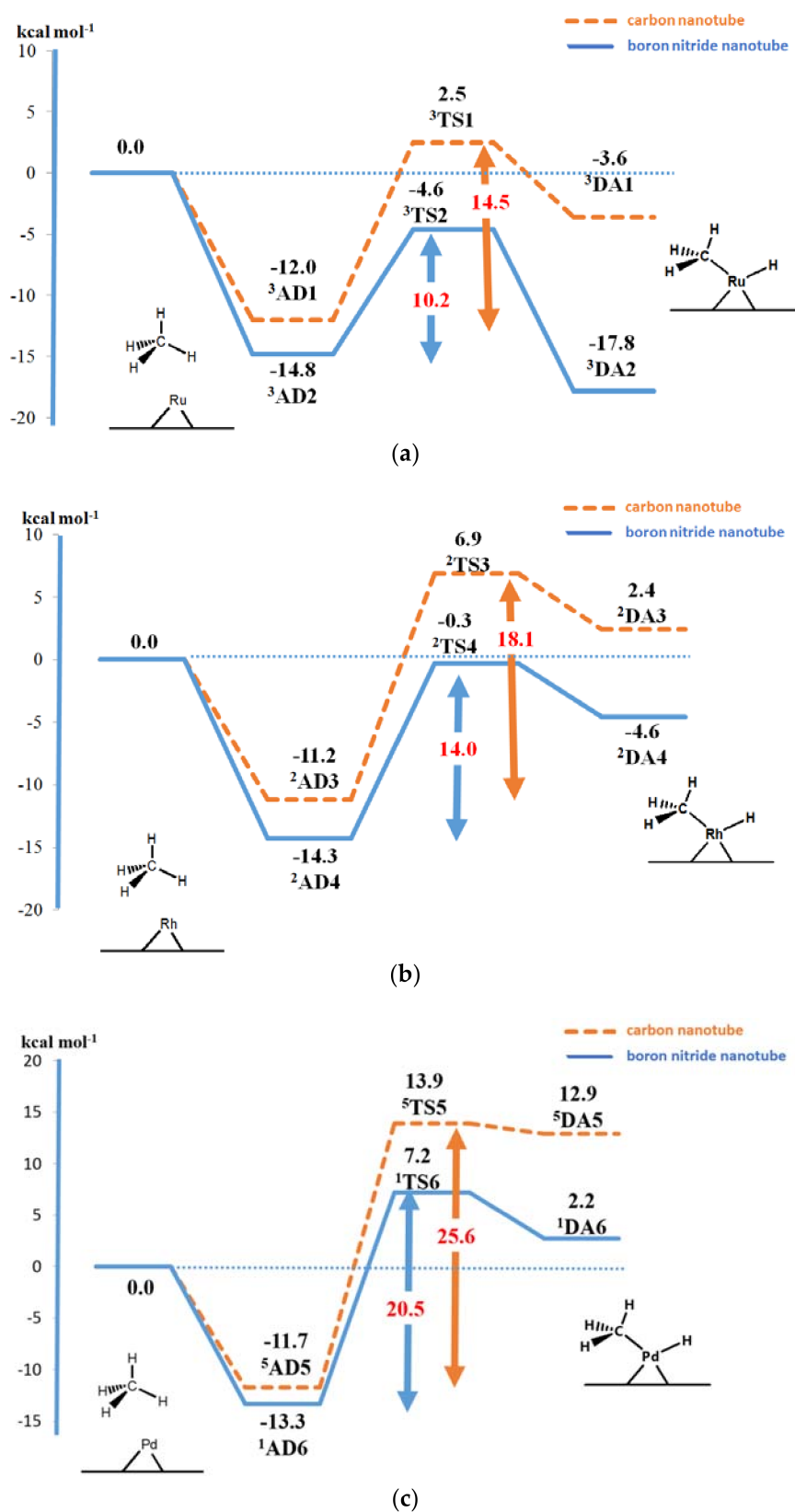
Figure 5. Energy profile for the methane dissociative adsorption reaction on the (**a**) Ru–, (**b**) Rh–, and (**c**) Pd–carbon nanotube and boron nitride nanotube with M06-L functional. Energies are in kcal mol^{-1}.

Our analyses on the dissociation of the adsorption complexes revealed endothermic reactions on the Ru–, Rh–, and Pd–carbon nanotube and the reverse activation energies were 6.1, 4.5, and 1.0 kcal mol^{-1}, respectively. The dissociation of the adsorption complex on the Pd–carbon nanotube was not very stable, especially when compared to that on the Ru– and Rh–carbon nanotube, and the reaction could revert back to the adsorption complex. For the boron nitride nanotube, the reactions on the Rh and Pd supports were found to be endothermic, whereas the reaction on the Ru support was exothermic. The reverse activation energies were 13.2, 4.3 and 5.0 kcal mol^{-1} on the Ru–, Rh–, and Pd–boron nitride nanotubes, respectively. Among all the decorated nanotubes examined in this study, the most thermodynamically favorable pathway for the dissociation of methane was found for the Ru–boron nitride nanotube (DA2), with a relative energy of -17.8 kcal mol^{-1}.

The Mulliken charge analysis (Table S3 in the supporting information) reveals different modes of electron transfer between the deposited metal and the supports. The carbon nanotube withdrew an electron from the metal atom, while the boron nitride nanotube donated an electron to the deposited metal. During the adsorption, an electron was transferred from methane to the metal-decorated nanotube. From the calculated transition states, we found that the anionic metal atom on boron nitride was responsible for the decreased activation energy of methane decomposition. In other words, the supported metal atom acted as the active center for the adsorption and dissociation of methane. Our results indicate that the supported Ru and Rd can activate the methane dissociation better than the supported Pd.

3. Models and Methods

In this study, a (8,0) carbon nanotube was chosen to be the support due to its outstanding physical and chemical properties [29]. The (8,0) carbon nanotube was represented by a 96-carbon cluster with 16 terminated hydrogen atoms. A monoatomic particle of Ru, Rh, or Pd was deposited separately on the outer surface of the carbon nanotube clusters, as shown in Figure 1a–c. The Ru–, Rh–, and Pd–C$_{96}$H$_{16}$ clusters were used to represent the metal-decorated carbon nanotube systems. The metal-supporting boron nitride nanotubes were generated in the same procedure. The Ru–, Rh–, and Pd–B$_{48}$N$_{48}$H$_{16}$ clusters in Figure 1d–f were used to represent the metal-decorated boron nitride nanotube systems.

Optimized structures of all metal/support clusters were determined by the DFT with M06-L functional [32] at ground state with various possible spin multiplicities. The M06 functional has been successfully applied to study the adsorption and catalytic reactions [36–39]. M06-L was previously used to investigate host–guest interactions on the carbon nanotube [40]. The method yielded the adsorption and activation energies of the bond dissociation reaction over metal catalysts that compared well with the most accurate coupled-cluster singles and doubles (CCSD) calculation [36]. All atoms were described by the 6–31G(d,p) basis set, except transition metal atoms, which were represented by the Stuttgart effective core potential functions [41]. We examined all the adsorption (AD), transition state (TS), and dissociative adsorption (DA) complexes corresponding to the proposed mechanism. For simplicity, the optimized structure (X) with spin multiplicity (S) was represented as ^{S}X.

During the structure optimization, all terminated hydrogen atoms were kept fixed to represent the constraint from extending structure. Optimized structures of all transition states were determined and confirmed by a single imaginary frequency, required to correspond with the reaction pathway. Transition states of each step were determined with the Berny algorithm [42]. The calculations were performed using the Gaussian 09 program [43].

4. Conclusions

The density functional theory has been applied to examine the decomposition of methane on the Ru-, Rh-, and Pd-decorated carbon nanotube and boron nitride nanotube catalysts. The C$_{96}$H$_{16}$ and B$_{48}$N$_{48}$H$_{16}$ clusters were optimized with M06-L functional. The adsorption energies of methane on the Ru–, Rh–, and Pd–carbon nanotubes were -12.0, -11.2, and -11.7 kcal mol^{-1}, respectively, while the corresponding total activation energies were 14.5, 18.1, and 25.6 kcal mol^{-1}, respectively.

The methane strongly adsorbed on the Ru–, Rh–, and Pd–boron nitride with adsorption energy of -14.8, -14.3, and -13.3 kcal mol^{-1}, respectively, while the activation energies were 10.2, 14.0, and 20.5 kcal mol^{-1}, respectively. The activities of the supported metals were in the order Ru > Rh > Pd and the supported metals performed better on boron–nitride nanotubes than on carbon nanotubes. The mechanism of the reactions with the Ru– or Rh–boron nitride nanotubes is preferable. These activation energies were lower than previous results for the metal supported on zeolite or silica or the metal surface. The changes in electron configuration of Ru and Rh atoms upon adsorption with nanotubes were found to play a significant role in the dissociative reaction mechanism.

Supplementary Materials: The following are available online at http://www.mdpi.com/2073-4344/8/5/190/s1, Table S1: The selected parameters of the adsorption, transition state, and dissociative adsorption complex on Ru-, Rh-, and Pd-decorated carbon nanotube with M06-L/6-31G(d,p) + Stuttgart basis set, Table S2: The selected parameters of the adsorption, transition state, and dissociative adsorption complex on Ru-, Rh-, and Pd-decorated boron nitride nanotubes with M06-L/6-31G(d,p) + Stuttgart basis set, Table S3: Mulliken charge |e| for the methane dissociative adsorption reaction on the Ru-, Rh- and Pd- carbon nanotube and Ru–, Rd–, and Pd–boron nitride nanotubes, Table S4: The relative energies (kcal mol^{-1}) of the adsorption and dissociative adsorption of methane on Ru-, Rh-, and Pd-decorated carbon nanotube and boron nitride nanotubes with M06-L/6-31G(d,p) + Stuttgart basis set.

References

1. Hammond, C.; Conrad, S.; Hermans, I. Oxidative methane upgrading. *ChemSusChem* **2012**, *5*, 1668–1686. [CrossRef] [PubMed]

2. Schwarz, H. Chemistry with methane: Concepts rather than recipes. *Angew. Chem. Int. Ed. Engl.* **2011**, *50*, 10096–10115. [CrossRef] [PubMed]

3. Wannakao, S.; Warakulwit, C.; Kongpatpanich, K.; Probst, M.; Limtrakul, J. Methane activation in gold cation-exchanged zeolites: A DFT study. *ACS Catal.* **2012**, *2*, 986–992. [CrossRef]

4. Alvarez-Galvan, M.C.; Mota, N.; Ojeda, M.; Rojas, S.; Navarro, R.M.; Fierro, J.L.G. Direct methane conversion routes to chemicals and fuels. *Catal. Today* **2011**, *171*, 15–23. [CrossRef]

5. Schwarz, H. Activation of Methane. *Angew. Chem. Int. Ed. Engl.* **1991**, *30*, 820–821. [CrossRef]

6. Shilov, A.E.; Shul'pin, G.B. Activation of C-H bonds by metal complexes. *Chem. Rev.* **1997**, *97*, 2879–2932. [CrossRef] [PubMed]

7. Impeng, S.; Khongpracha, P.; Warakulwit, C.; Jansang, B.; Sirijaraensre, J.; Ehara, M.; Limtrakul, J. Direct oxidation of methane to methanol on Fe-O modified graphene. *RSC Adv.* **2014**, *4*, 12572–12578. [CrossRef]

8. Panov, G.I.; Sobolev, V.I.; Dubkov, K.A.; Parmon, V.N.; Ovanesyan, N.S.; Shilov, A.E.; Shteinman, A.A. Iron complexes in zeolites as a new model of methane monooxygenase. *React. Kinet. Catal. Lett.* **1997**, *61*, 251–258. [CrossRef]

9. Pantu, P.; Pabchanda, S.; Limtrakul, J. Theoretical investigation of the selective oxidation of methane to methanol on nanostructured Fe-ZSM-5 by the ONIOM method. *ChemPhysChem* **2004**, *5*, 1901–1906. [CrossRef] [PubMed]

10. Hu, X.; Li, H.; Wu, T. Approaching and bond breaking energies in the C-H activation and their application in catalyst design. *J. Phys. Chem. A* **2011**, *115*, 904–910. [CrossRef] [PubMed]

11. Latimer, A.A.; Aljama, H.; Kakekhani, A.; Yoo, J.S.; Kulkarni, A.; Tsai, C.; Garcia-Melchor, M.; Abild-Pedersen, F.; Nørskov, J.K. Mechanistic insights into heterogeneous methane activation. *Phys. Chem. Chem. Phys.* **2017**, *19*, 3575–3581. [CrossRef] [PubMed]

12. Baughman, R.H.; Zakhidov, A.A.; De Heer, W.A. Carbon nanotubes—The route toward applications. *Science* **2002**, *297*, 787–792. [CrossRef] [PubMed]

13. Iijima, S.; Ichihashi, T. Single-shell carbon nanotubes of 1-nm diameter. *Nature* **1993**, *363*, 603–605. [CrossRef]

14. Stankovich, S.; Dikin, D.A.; Dommett, G.H.B.; Kohlhaas, K.M.; Zimney, E.J.; Stach, E.A.; Piner, R.D.; Nguyen, S.T.; Ruoff, R.S. Graphene-based composite materials. *Nature* **2006**, *442*, 282–286. [CrossRef] [PubMed]

15. Thostenson, E.T.; Ren, Z.; Chou, T.W. Advances in the science and technology of carbon nanotubes and their composites: A review. *Compos. Sci. Technol.* **2001**, *61*, 1899–1912. [CrossRef]

16. Wildgoose, G.G.; Banks, C.E.; Compton, R.G. Metal nanoparticles and related materials supported on Carbon nanotubes: Methods and applications. *Small* **2006**, *2*, 182–193. [CrossRef] [PubMed]

17. Peng, X.; Chen, J.; Misewich, J.A.; Wong, S.S. Carbon nanotube-nanocrystal heterostructures. *Chem. Soc. Rev.* **2009**, *38*, 1076–1098. [CrossRef] [PubMed]

18. Planeix, J.M.; Coustel, N.; Coq, B.; Brotons, V.; Kumbhar, P.S.; Dutartre, R.; Geneste, P.; Bernier, P.; Ajayan, P.M. Application of Carbon Nanotubes as Supports in Heterogeneous Catalysis. *J. Am. Chem. Soc.* **1994**, *116*, 7935–7936. [CrossRef]

19. Ye, X.R.; Lin, Y.; Wang, C.; Engelhard, M.H.; Wang, Y.; Wai, C.M. Supercritical fluid synthesis and characterization of catalytic metal nanoparticles on carbon nanotubes. *J. Mater. Chem.* **2004**, *14*, 908–913. [CrossRef]

20. Zhang, X.Q.; Li, H.; Liew, K.M. The structures and electrical transport properties of germanium nanowires encapsulated in carbon nanotubes. *J. Appl. Phys.* **2007**, *102*, 073709. [CrossRef]

21. Leghrib, R.; Dufour, T.; Demoisson, F.; Claessens, N.; Reniers, F.; Llobet, E. Gas sensing properties of multiwall carbon nanotubes decorated with rhodium nanoparticles. *Sens. Actuator B-Chem.* **2011**, *160*, 974–980. [CrossRef]

22. Li, Y.; Wang, H.; Chen, Y.; Yang, M. A multi-walled carbon nanotube/palladium nanocomposite prepared by a facile method for the detection of methane at room temperature. *Sens. Actuator B-Chem.* **2008**, *132*, 155–158. [CrossRef]

23. Star, A.; Joshi, V.; Skarupo, S.; Thomas, D.; Gabriel, J.C.P. Gas sensor array based on metal-decorated carbon nanotubes. *J. Phys. Chem. B* **2006**, *110*, 21014–21020. [CrossRef] [PubMed]

24. Vermisoglou, E.C.; Romanos, G.E.; Karanikolos, G.N.; Kanellopoulos, N.K. Catalytic NO_x removal by single-wall carbon nanotube-supported Rh nanoparticles. *J. Hazard. Mater.* **2011**, *194*, 144–155. [CrossRef] [PubMed]

25. Wang, X.; Yuan, Q.; Li, J.; Ding, F. The transition metal surface dependent methane decomposition in graphene chemical vapor deposition growth. *Nanoscale* **2017**, *9*, 11584–11589. [CrossRef] [PubMed]

26. Bunnik, B.S.; Kramer, G.J. Energetics of methane dissociative adsorption on Rh{111} from DFT calculations. *J. Catal.* **2006**, *242*, 309–318. [CrossRef]

27. Li, Y.; Lu, X.; Li, Y.; Zhang, X. Oxygen evolution reaction in nanoconfined carbon nanotubes. *Phys. E Low-Dimens. Syst. Nanostruct.* **2018**, *99*, 1–5. [CrossRef]

28. Zhao, C.; Wu, H. A first-principles study on the interaction of biogas with noble metal (Rh, Pt, Pd) decorated nitrogen doped graphene as a gas sensor: A DFT study. *Appl. Surf. Sci.* **2018**, *435*, 1199–1212. [CrossRef]

29. Luna, C.R.; Verdinelli, V.; Germán, E.; Seitz, H.; Volpe, M.A.; Pistonesi, C.; Jasen, P.V. Hydrogen adsorption and associated electronic and magnetic properties of Rh-decorated (8,0) carbon nanotubes using Density Functional Theory. *J. Phys. Chem. C* **2015**, *119*, 13238–13247. [CrossRef]

30. Chopra, N.G.; Luyken, R.J.; Cherrey, K.; Crespi, V.H.; Cohen, M.L.; Louie, S.G.; Zettl, A. Boron nitride nanotubes. *Science* **1995**, *269*, 966–967. [CrossRef] [PubMed]

31. Ritleng, V.; Sirlin, C.; Pfeffer, M. Ru-, Rh-, and Pd-catalyzed C-C bond formation involving C-H activation and addition on unsaturated substrates: Reactions and mechanistic aspects. *Chem. Rev.* **2002**, *102*, 1731–1769. [CrossRef] [PubMed]

32. Zhao, Y.; Truhlar, D.G. The M06 suite of density functionals for main group thermochemistry, thermochemical kinetics, noncovalent interactions, excited states, and transition elements: Two new functionals and systematic testing of four M06-class functionals and 12 other functionals. *Theor. Chem. Acc.* **2008**, *120*, 215–241. [CrossRef]

33. Robertson, D.H.; Brenner, D.W.; Mintmire, J.W. Energetics of nanoscale graphitic tubules. *Phys. Rev. B* **1992**, *45*, 12592–12595. [CrossRef]

34.　Carstens, J.N.; Bell, A.T. Methane activation and conversion to higher hydrocarbons on supported ruthenium. *J. Catal.* **1996**, *161*, 423–429. [CrossRef]

35.　Stewart, C.N.; Ehrlich, G. Dynamics of activated chemisorption: Methane on rhodium. *J. Chem. Phys.* **1975**, *62*, 4672–4682. [CrossRef]

36.　Boekfa, B.; Pahl, E.; Gaston, N.; Sakurai, H.; Limtrakul, J.; Ehara, M. C-Cl bond activation on Au/Pd bimetallic nanocatalysts studied by density functional theory and genetic algorithm calculations. *J. Phys. Chem. C* **2014**, *118*, 22188–22196. [CrossRef]

37.　Boekfa, B.; Pantu, P.; Probst, M.; Limtrakul, J. Adsorption and tautomerization reaction of acetone on acidic zeolites: The confinement effect in different types of zeolites. *J. Phys. Chem. C* **2010**, *114*, 15061–15067. [CrossRef]

38.　Pornsatitworakul, S.; Boekfa, B.; Maihom, T.; Treesukol, P.; Namuangruk, S.; Jarussophon, S.; Jarussophon, N.; Limtrakul, J. The coumarin synthesis: A combined experimental and theoretical study. *Monatsh. Chem.* **2017**, *148*, 1245–1250. [CrossRef]

39.　Maitarad, P.; Namuangruk, S.; Zhang, D.; Shi, L.; Li, H.; Huang, L.; Boekfa, B.; Ehara, M. Metal-porphyrin: A potential catalyst for direct decomposition of N_2O by theoretical reaction mechanism investigation. *Environ. Sci. Technol.* **2014**, *48*, 7101–7110. [CrossRef] [PubMed]

40.　Zhao, Y.; Truhlar, D.G. Size-selective supramolecular chemistry in a hydrocarbon nanoring. *J. Am. Chem. Soc.* **2007**, *129*, 8440–8442. [CrossRef] [PubMed]

41.　Bergner, A.; Dolg, M.; Küchle, W.; Stoll, H.; Preuß, H. Ab initio energy-adjusted pseudopotentials for elements of groups 13–17. *Mol. Phys.* **1993**, *80*, 1431–1441. [CrossRef]

42.　Gonzalez, C.; Bernhard Schlegel, H. An improved algorithm for reaction path following. *J. Chem Phys.* **1989**, *90*, 2154–2161. [CrossRef]

43.　Frisch, M.J.; Trucks, G.W.; Schlegel, H.B.; Scuseria, G.E.; Robb, M.A.; Cheeseman, J.R.; Scalmani, G.; Barone, V.; Petersson, G.A.; Nakatsuji, H.; et al. *Gaussian 09 Revision D.01*; Gaussian Inc.: Wallingford, CT, USA, 2009.